MODELING AND SIMULATION OF BUBBLING FLUIDIZED BEDS CONTAINING PARTICLE MIXTURES

D. Lathouwers and J. Bellan†

Jet Propulsion Laboratory, California Institute of Technology, Pasadena, CA. 91109-8099

Word Count: 5960 (Introduction 473, Model 1905, Results 1301, Conclusions 269, equations 588, References 168, acknowledgment 56, figures 1200)

†Corresponding author: Dr. J. Bellan

Jet Propulsion Laboratory

California Institute of Technology

MS. 125-109

4800 Oak Grove Drive

Pasadena, CA 91109

USA

Tel: (818) 354-6959

Fax: (818) 393-5011

Email: Josette.Bellan@jpl.nasa.gov

Colloquium: Combustion of Solid Fuels, PF, FBC, and Waste Incineration.

Oral presentation

ABSTRACT

A comprehensive model is presented for mathematically describing the isothermal, non-reactive, fluid dynamics of a mixture of particles in a gas. A multifluid approach is followed where macroscopic transport equations are derived by taking suitable ensemble averages of the local gas and particle dynamic equations. A standard phasic ensemble average is selected for the gas phase, whereas the particle equations are derived using a kinetic theory approach where collisional transfer is included. Separate transport equations are constructed for each of the particle classes, allowing for the description of the independent acceleration of the particles in each class and the equilibration processes whereby momentum and energy are exchanged between each class, leading to a wider range of applicability than common mixture equations. Closure of the particle equations is exercised by providing separate velocity distributions for each of the particle classes, here specified as Gaussian; this being a valid approach for small gradients in the mean variables, and for nearly elastic particles. In the region of very high solids volume fractions, the relations obtained for the stress tensor are augmented by a model describing frictional transfer. The model is applied to three different testcases: i) prediction of the shear and normal stresses in a homogeneous shear flow, ii) simulation of the particle pressure along the wall of a bubbling bed, and iii) a comparison between simulations of monodisperse and binary mixtures in a homogeneously aerated bed. Where possible, the comparison between simulations and available experimental data is reasonable.

1 INTRODUCTION

Fluidized bed reactors containing a granular mixture of sand (carrier) and biomass particles, fluidized by steam, are considered promising for commercial operation. Since numerical simulations constitute a cost-effective tool to optimize the operation of such reactors, the focus is here on a model for the hydrodynamic prediction of such granular mixtures.

Experiments indicate that in a rapidly sheared granular flow, momentum and energy are exchanged in particle collisions rather than in enduring frictional contacts or through the interstitial gas. The particles then interact similarly to molecules of a dense gas. Important differences among the two systems include the occurrence of dissipation due to the inelasticity of particle-particle collisions and the fact that continuum time and length scales involve far less collisions and particle diameters, respectively. Jenkins and Richman [1] first exploited this analogy and used a kinetic theory approach to derive macroscopic equations of the mixture. Their theory was based on a Gaussian velocity distribution function, and has since been improved by considering more general velocity distributions [2][3], and by including effects of the interstitial gas (e.g. [4]). A crucial role in these theories is played by the 'granular temperature', the mean kinetic energy associated with the velocity fluctuations of the particles. At higher solid fractions or at lower shear rates, particle-particle friction becomes the dominant mechanism of momentum transfer and the equations must be augmented by a frictional stress model, usually based on empirical constitutive laws, as in soil mechanics. After the pioneering work of Ding and Gidaspow [5], granular flow theories are now commonly applied in the field of hydrodynamic prediction of bubbling and circulating fluidized bed systems.

The focus is here on the description of a binary particle mixture consisting of sand and biomass. These particles will, in general, have different properties (density, diameter), and this may lead

to flow-induced segregation. Analysis of binary (or multicomponent) dry granular mixtures are available [6],[7],[8],[9], but these all assume the granular temperature of the constituents to be equal, this being a reasonable assumption in the absence of external driving forces and for a mass ratio near unity. Furthermore, all aforementioned studies derive *mixture* equations for mass, momentum, and energy, augmented by algebraic relations for the drift velocities of the constituents, assuming equilibrium. Koch [10] shows that these conditions are not necessarily met in the presence of an interstitial gas.

Here we derive a comprehensive model for the flow of a multicomponent particle mixture, based on separate dynamic equations for each particle class with interaction terms describing the various equilibration processes. The kinetic theory is based on the Gaussian approximation assuming the spatial gradients of the mean variables to be small and the particles to be nearly elastic. The resulting closure relations are extensively discussed. The combined gas-particle multifluid model is applied to a number of flows in order to evaluate its quantitative predictive capabilities.

2 MODEL

A continuum model is derived by applying separate averaging procedures for both gas and solids. A phase ensemble average is used for the continuous phase, combined with a particle ensemble average where particle properties, such as linear velocity, are directly averaged.

2.1 Gas phase transport equations

As phasic ensemble averaging is a well-known procedure (cf. [11]), we will only list the major steps. The general ensemble average of a field quantity $\Psi(\mathbf{x}, t)$, ($\mathbf{x}, t$ denoting space and time coordinates)

is

$$< \Psi(\mathbf{x},t) >= \int \Psi(\mathbf{x},t) P(\omega) d\omega \tag{1}$$

where $P(\omega)$ is the probability that a specific realization ω is encountered in the ensemble. The gas-phase ensemble average and its density-weighted counterpart are defined as $\overline{\Psi} =< \chi_g \Psi(\mathbf{x},t) > /\alpha_g$ and $\widetilde{\Psi} =< \chi_g \rho_g \Psi(\mathbf{x},t) > /\alpha_g \overline{\rho}_g$, where ρ_g is the gas density, χ_g denotes the phase indicator of the gas phase which is unity in the gas phase and zero otherwise, and the gas phase fraction, α_g, is defined as the ensemble average of the indicator function, i.e. $< \chi_g >$. The average transport equations for the gas phase now follow by multiplying the local instantaneous equations of mass and momentum conservation by the phase indicator and applying the ensemble averaging operator. The result is

$$\frac{\partial \alpha_g \overline{\rho}_g}{\partial t} + \nabla \cdot \alpha_g \overline{\rho}_g \widetilde{\mathbf{u}}_g = 0 \tag{2}$$

$$\frac{\partial \alpha_g \overline{\rho}_g \widetilde{\mathbf{u}}_g}{\partial t} + \nabla \cdot \alpha_g \overline{\rho}_g \widetilde{\mathbf{u}}_g \widetilde{\mathbf{u}}_g = \nabla \cdot [\alpha_g \overline{\boldsymbol{\sigma}}_g + \boldsymbol{\Sigma}_g^{Re}] + \alpha_g \overline{\rho}_g \mathbf{g} + \mathbf{M}_g \tag{3}$$

Here, $\overline{\boldsymbol{\sigma}}_g$ represents the average stress tensor, $\boldsymbol{\Sigma}_g^{Re}$ the 'turbulent' stress tensor defined as $- < \chi_g \rho_g \mathbf{u}_g' \mathbf{u}_g' > /\alpha_g$ which results from fluctuations (indicated by a prime) on the mean $\mathbf{u}' = \mathbf{u} - \widetilde{\mathbf{u}}$, and $\mathbf{M}_g = - < \boldsymbol{\sigma}_g \cdot \nabla \chi_g >$ is the average phase interaction with the particles. In the above derivation we have neglected mass transfer between the particles and the gas, as here we treat only the isothermal, non-reactive case. It is customary to rewrite the momentum equation as ([11])

$$\frac{\partial \alpha_g \overline{\rho}_g \widetilde{\mathbf{u}}_g}{\partial t} + \nabla \cdot \alpha_g \overline{\rho}_g \widetilde{\mathbf{u}}_g \widetilde{\mathbf{u}}_g = -\alpha_g \nabla \overline{p}_g + \nabla \cdot [\alpha_g \overline{\boldsymbol{\tau}}_g + \boldsymbol{\Sigma}_g^{Re}] + \alpha_g \overline{\rho}_g \mathbf{g} + \mathbf{M}_g' \tag{4}$$

where $\overline{\boldsymbol{\tau}}_g$ is the average viscous stress tensor and $\mathbf{M}_g'$ represents the combined effect of drag, added mass, etc. on the gas. The above equations require closure relations for $\overline{p}_g$, $\overline{\boldsymbol{\tau}}_g$, $\boldsymbol{\Sigma}_g^{Re}$, and $\mathbf{M}_g'$. Here we neglect gas phase turbulence effects and therefore ignore $\boldsymbol{\Sigma}_g^{Re}$. A detailed turbulence model derivation for the general reactive case can be found in [12]. The average gas pressure

is rigorously related to the average gas density by applying the ensemble averaging operator to the perfect gas law, i.e. $\overline{p}_g = \overline{\rho}_g RT$. The average viscous stress tensor is approximated by a form similar to its microscopic counterpart $\overline{\tau}_g = 2\mu_g \mathbf{S}_g$, where $\mathbf{S}$ denotes the strain rate tensor: $\mathbf{S} = (\nabla \mathbf{u} + \nabla \mathbf{u}^T)/2 - (\nabla \cdot \mathbf{u})/3$. Closure of the average momentum transfer between the phases is derived below.

2.2 Particle phase transport equations

The transport equations are derived similarly to those for dense gases, using kinetic theory concepts. An important difference from classical kinetic theory occurs due to the inelasticity of collisions between macroscopic particles leading to dissipation. Furthermore, an interstitial gas exerts drag on the particles, leading to interaction terms in the averaged transport equations.

While a considerable literature exists on the development of equations of motion for multicomponent mixtures, most of it is restricted to the case where the temperatures and velocities of the species are nearly equal and evolve according to the dynamic equations of the mixture. This classical mixture theory [13] requires that $\Delta u/\Theta_c << 1$ (Δu being a characteristic relative velocity of the particle classes and Θ_c a characteristic rms velocity, i.e. temperature), a condition not necessarily satisfied in granular flows. Therefore, here we derive separate dynamic equations for each of the particle classes, similar to that of Goldman and Sirovich [14] for a dilute mixture of interacting species. Here, a similar procedure is implemented for a dense suspension of hard spheres (cf. [10]). The dynamic evolution of these systems is governed by an appropriate set of Boltzmann equations

$$\frac{\partial f_i^{(1)}}{\partial t} + \frac{\partial}{\partial \mathbf{x}}[\mathbf{c}_i f_i^{(1)}] + \frac{\partial}{\partial \mathbf{c}_i}[\frac{\mathbf{F}_i}{m_i} f_i^{(1)}] = \sum_j J_{ij} \tag{5}$$

where $f_i^{(1)}$ is the single particle distribution function of species i, $\mathbf{F}_i$ is the external force on the particle (i.e. gravity and gas-particle drag), and m_i and $\mathbf{c}_i$ are the mass and velocity of the particle,

respectively. The right hand side represents the effect of collisions with particles of all classes on the distribution function. Average particle properties are then derived from $f_i^{(1)}$:

$$< \Psi(\mathbf{x},t) >_i = \frac{1}{n_i} \int \Psi f_i^{(1)} d\mathbf{c} \tag{6}$$

where n_i is the number density of the class-i particles; $n_i = \int f_i^{(1)} d\mathbf{c}$. Defining $\alpha_i \rho_i = n_i m_i$, $\mathbf{u}_i =< \mathbf{c} >_i$, $\mathbf{C}_i = \mathbf{c}_i - \mathbf{u}_i$, and $\Theta_i = \frac{1}{3} < C^2 >_i$, where α_i denotes the particle phase fraction, $\mathbf{u}_i$ is the mean velocity, $\mathbf{C}_i$ is the fluctuating velocity, and Θ_i the granular temperature. The moment equations are derived by multiplying the Boltzmann equation by a variable Ψ and integrating over velocity space. The general transport equation obtained is

$$\frac{\partial \alpha_i \rho_i < \Psi >_i}{\partial t} + \nabla \cdot \alpha_i \rho_i \mathbf{u}_i < \Psi >_i = \sum_k [\chi_{ik}(m_i \Psi_i) - \nabla \cdot \theta_{ik}(m_i \Psi_i)] + \alpha_i \rho_i < \frac{\mathbf{F}_i}{m_i} \frac{\partial \Psi_i}{\partial \mathbf{c}_i} >_i . \tag{7}$$

Here, χ_{ik} denotes a collisional source and θ_{ik} represents a collisional flux, resulting from all types of collisions. The form of these collisional integrals is given in [7]. These integrals involve the complete pair distribution function $f_{ik}^{(2)}(\mathbf{c}_1, \mathbf{r} - 1/2\sigma_{ik}\mathbf{k}, \mathbf{c}_2, \mathbf{r} + 1/2\sigma_{ik}\mathbf{k})$ which gives the probability of finding a pair of spheres such that particle 1 of class i is located at $\mathbf{r} - 1/2\sigma_{ik}\mathbf{k}$ with velocity $\mathbf{c}_1$ and particle 2 of class k is at $\mathbf{r} + 1/2\sigma_{ik}\mathbf{k}$ with velocity $\mathbf{c}_2$, where $\mathbf{k}$ is the unit vector directed from the center of particle 1 to that of particle 2 at the moment of collision, and $\sigma_{ik} = \sigma_i + \sigma_k$, is the sum of the radii of the two spheres.

By substituting Ψ with 1, $\mathbf{c}_i$, and $1/2c_i^2$, we obtain mass conservation, momentum conservation, and conservation of granular 'turbulent' energy equations:

mass:

$$\frac{\partial \alpha_i \rho_i}{\partial t} + \nabla \cdot \alpha_i \rho_i \mathbf{u}_i = 0, \tag{8}$$

momentum:

$$\frac{\partial \alpha_i \rho_i \mathbf{u}_i}{\partial t} + \nabla \cdot \alpha_i \rho_i \mathbf{u}_i \mathbf{u}_i = -\nabla \cdot \mathbf{\Sigma}_i + \boldsymbol{\phi}_i + \alpha_i \rho_i < \frac{\mathbf{F}}{m} >_i \tag{9}$$

where $\mathbf{\Sigma}_i = \alpha_i \rho_i < \mathbf{CC} >_i + \sum_k \theta_{ik}(m_i \mathbf{C}_i)$ represents the effective stress tensor of the particles consisting of a kinetic contribution (first term) and contributions originating from collisions with particles of all classes (second term). $\boldsymbol{\phi}_i = \sum_k \chi_{ik}(m_i \mathbf{C}_i)$ is the collisional source term resulting from collisions between unlike particles. The final term in the equation denotes the average force exerted on the particles by drag.

granular temperature:

$$\frac{3}{2}\left[\frac{\partial \alpha_i \rho_i \Theta_i}{\partial t} + \nabla \cdot \alpha_i \rho_i \mathbf{u}_i \Theta_i\right] = -\mathbf{\Sigma}_i : \nabla \mathbf{u}_i - \nabla \cdot \mathbf{q}_i + \gamma_i + \alpha_i \rho_i < \frac{\mathbf{F}}{m} \cdot \mathbf{C} >_i . \tag{10}$$

The first term on the right hand side is the production of granular temperature by shearing of the particles. $\mathbf{q}_i = \alpha_i \rho_i < 1/2 C^2 \mathbf{C} >_i + \sum_k \theta_{ik}(1/2 m_i C_i^2)$ is the average 'heat flux' both due to velocity fluctuations themselves (first term) and through collisions (second term). The source term $\gamma_i = \sum_k \chi_{ik}(1/2 m_i C_i^2)$ represents the effects of redistribution of energy among particle classes and the dissipative effect of inelastic collisions. The final term incorporates the effect of fluid-particle drag on the energy balance; depending on the situation, this may be either a source or sink.

2.2.1 Closure

The previously derived model describes the dynamics using conservation equations for mass, momentum and granular temperature of each solids class. These multiple-class equations can describe the independent accelerations of the species, as well as momentum and energy exchange between solids classes. Moreover, these transport equations are valid even when Δu is of the same order as Θ_c.

To obtain closure of the equations, we need to specify the dynamics of collisions and the complete

pair distribution function $f_{ik}^{(2)}$ for the calculation of the collisional terms χ_{ik} and θ_{ik}. Furthermore, to model the exchange terms with the gas phase, $\mathbf{F}_i$ needs to be specified.

Collision dynamics Assuming exclusively binary collisions and that the particles are perfectly spherical and smooth, the relation between the velocities of the particles right before and after a collision of particle 1 of class i and particle 2 of class k is determined from the conservation of linear momentum and energy [13]. Defining $\mathbf{l}$ as the relative velocity, $\mathbf{c}_1 - \mathbf{c}_2$, we assume $\mathbf{l}$ before and after collision to be related as $(\mathbf{l}' \cdot \mathbf{k}) = -e_{ik}(\mathbf{l} \cdot \mathbf{k})$, where e_{ik} is the restitution coefficient, incorporating the effect of inelasticity on the collisions ($e_{ik} = 1$ for perfectly elastic encounters). Therefore, $\mathbf{c}_1' - \mathbf{c}_1' = -M_k(1 + e_{ik})(\mathbf{l} \cdot \mathbf{k})\mathbf{k}$, where $M_k = m_k/(m_i + m_k)$ is the reduced mass. Thus, the exchange $\Psi_i' - \Psi_i$ of any particle property Ψ_i is a function of $\mathbf{l}$, $\mathbf{k}$ and the center of mass velocity, $\mathbf{c}_m = M_i\mathbf{c}_1 + M_k\mathbf{c}_2$.

Particle dynamics The momentum equation of a single particle can be approximated as

$$m_i \frac{d\mathbf{c}_i}{dt} = \mathbf{F}_i = m_i\mathbf{g} - V_i\nabla\widehat{p}_g + \frac{m_i}{\tau_{i,12}}(\widehat{\mathbf{u}}_g - \mathbf{c}_i) \tag{11}$$

where the total force on the particle is due to gravity, gas pressure gradient and gas-particle drag. V_i is the volume of the particle and $\tau_{i,12}$ represents the relaxation time scale of the particle. The $\widehat{()}$ on the gas-phase variables denotes the location of the particle, as if the surrounding flow was undisturbed by its presence [4]. The gas-particle interaction time scale depends strongly on the flow regime; in the dilute regime it is derived from the drag coefficient, C_d, of a single particle in an infinite medium, empirically corrected for the presence of other surrounding particles by a function $f(\alpha_g) = \alpha_g^{-1.7}$ (e.g. [15]) whereas in the dense regime the classical Ergun relation is used. To avoid discontinuous behavior, a weighted average of the two time scales is introduced

$$\frac{1}{\tau_{i,12}} = W\frac{3\rho_g C_d(Re_i)}{4\rho_i d_i}|\mathbf{c}_i - \widehat{\mathbf{u}}_g|f(\alpha_g) + (1 - W)\frac{\rho_g}{\rho_i}\left[(1 - \alpha_g)\frac{150}{Re_i} + 1.75\right]\frac{|\mathbf{c}_i - \widehat{\mathbf{u}}_g|}{d_i} \tag{12}$$

where the present switch function, $W(\alpha_g) = \arctan(150(\alpha_g - 0.8))/\pi + 1/2$, gives a rapid transition from one regime to the other. d_i is the diameter of the particle and Re_i the Reynolds number based on the relative velocity with the gas.

In order to calculate the collisional integrals, a definitive form for the complete pair distribution function is required. As in dense gas theory, Enskog's method is employed to account for the correlations in the positions of a pair of particles just prior to collision. Here, $h_{ik}(\mathbf{r})$ is the radial distribution function at contact, accounting for the effects of excluded area and particle shielding on the spatial distribution of colliding pairs. Its form is taken from [7], slightly adjusted to prevent overpacking of the solids

$$h_{ik} = \frac{1}{1-\alpha/\alpha_0} + 6\frac{\sigma_i\sigma_k}{\sigma_i+\sigma_k}\frac{\xi}{(1-\alpha/\alpha_0)^2} + 8\left(\frac{\sigma_i\sigma_k}{\sigma_i+\sigma_k}\right)^2\frac{\xi}{(1-\alpha/\alpha_0)^2} \tag{13}$$

where α denotes the total particle volume fraction and $\xi = 2\pi/3\sum n_i\sigma_i^2$. The single particle distribution functions are solutions of (5), here assumed to be Gaussian

$$f_i^{(1)}(\mathbf{c},\mathbf{r},t) = \frac{n_i}{(2\pi\Theta_i)^{3/2}}\exp[-\frac{(\mathbf{c}-\mathbf{u}_i)^2}{2\Theta_i}]. \tag{14}$$

This is a good approximation if spatial gradients of the mean fields are small and the spheres are nearly elastic. Using the above distributions and neglecting products of the spatial gradients, products of $(1-e_{ik})$ with the spatial gradients, and products of Δu with the spatial gradients yields the following constitutive equations for $\boldsymbol{\phi}_i$, $\boldsymbol{\Sigma}_i$, $\mathbf{q}_i$, and γ_i:

$$\boldsymbol{\phi}_i = \sum_k \frac{1}{3}F_{ik}\left\{\pi(\Theta_i+\Theta_k)^{1/2}(\mathbf{u}_k-\mathbf{u}_i) + 4\sqrt{2\pi}\sigma_{ik}(\Theta_i+\Theta_k)\nabla\ln\frac{n_i}{n_k}\right\} \tag{15}$$

$$\boldsymbol{\Sigma}_i = n_i m_i\Theta_i + \sum_k p_{ik}\mathbf{I} - \mu_i^i[2\mathbf{S}_i + \frac{5}{3}\nabla\cdot\mathbf{u}_i] - \mu_i^k[2\mathbf{S}_k + \frac{5}{3}\nabla\cdot\mathbf{u}_k] \tag{16}$$

$$\mathbf{q}_i = \sum_k \kappa_i^i\nabla\Theta_i + \kappa_i^k\nabla\Theta_k \tag{17}$$

$$\gamma_i = \sum_k -2\sqrt{2\pi}F_{ik}(\Theta_i+\Theta_k)^{1/2}\{2(M_i\Theta_i - M_k\Theta_k) + M_k(1-e_{ik})(\Theta_i+\Theta_k)\} \tag{18}$$

where $F_{ik} = n_i n_k m_i M_k (1 + e_{ik}) h_{ik} \sigma_{ik}^2$. The pressure and transport coefficients are given by

$$p_{ik} = \frac{1}{3}\pi n_i n_k m_i M_k (1 + e_{ik}) h_{ik} \sigma_{ik}^3 (\Theta_i + \Theta_k) \tag{19}$$

$$\mu_i^i = \frac{1}{15}\sqrt{2\pi} n_i n_k m_i M_k^2 (1 + e_{ik}) h_{ik} \sigma_{ik}^4 (\Theta_i + \Theta_k)^{3/2} / \Theta_i \tag{20}$$

$$\mu_i^k = \frac{1}{15}\sqrt{2\pi} n_i n_k m_k M_i^2 (1 + e_{ik}) h_{ik} \sigma_{ik}^4 (\Theta_i + \Theta_k)^{3/2} / \Theta_k \tag{21}$$

$$\kappa_i^i = \frac{1}{3}\sqrt{2\pi} n_i n_k m_i M_k (1 + e_{ik}) h_{ik} \sigma_{ik}^4 (\Theta_i + \Theta_k)^{1/2} (M_k \Theta_k / \Theta_i) \tag{22}$$

$$\kappa_i^k = \frac{1}{3}\sqrt{2\pi} n_i n_k m_i M_k (1 + e_{ik}) h_{ik} \sigma_{ik}^4 (\Theta_i + \Theta_k)^{1/2} (M_i \Theta_i / \Theta_k) \tag{23}$$

The terms in $\boldsymbol{\phi_i}$ represent solid-solid drag and ordinary diffusion, respectively (thermal diffusion has been neglected). The stress tensor depends on the shear rates of all solid classes where the shear viscosities arise entirely from collisions, not from streaming (Gaussian approximation). Similar remarks hold for the heat flux vector. The source terms in the granular energy equations contain two terms: a temperature equilibrating and a dissipative term.

To complete model closure, the coupling terms between gas and solids require specification. For the momentum equation we use

$$\alpha_i \rho_i < \frac{\mathbf{F}_i}{m_i} >_i = \alpha_i \rho_i \mathbf{g} - \alpha_i \rho_i < \frac{V_i}{m_i} \nabla \widehat{p}_g + \frac{1}{\tau_{i,12}} (\widehat{\mathbf{u}}_g - \mathbf{c}_i) >_i \simeq \alpha_i \rho_i \mathbf{g} - \alpha_i \nabla \overline{p}_g - \frac{\alpha_i \rho_i}{\tau_{i,12}} (\mathbf{u}_i - \widetilde{\mathbf{u}}_g) \tag{24}$$

where fluctuations in the gas-phase variables have been neglected. For consistency between the gas and solids equations, $\mathbf{M}_g' = \sum_i \frac{\alpha_i \rho_i}{\tau_{i,12}} (\mathbf{u}_i - \widetilde{\mathbf{u}}_g)$. In Eq. (10), the coupling term is neglected which is a good approximation in the case of heavy particles (large $\tau_{i,12}$).

The constitutive equations are restricted to the region where particles interact exclusively through slightly inelastic, short duration, collisions. However, as the volumetric fraction approaches α_0, particles will, increasingly, be in simultaneous contact with several neighbors and stresses will be transmitted at points of sustained sliding or rolling contact. This situation is very difficult to treat at the microscopic level, leading to its neglect in many bubbling fluidized bed models. However,

in certain regions where shear rates are very small, the granular temperature may be too small to support the solids phase. Hence, these codes require a 'numerical fix', generally restricting the computed granular temperature (e.g. [16],[17]). To avoid this situation, we explicitly model the frictional regime, particularly since it was shown in [18] that inclusion of the frictional regime is necessary for obtaining qualitatively correct behavior of granular flow.

The approach followed is similar to that used in [19], extended here for the case of multiple particle classes. The model proposed attains a simple relation between stresses and strains

$$\boldsymbol{\sigma}_i^f = -p_i^f \mathbf{I} + 2\mu_i^f \mathbf{S}_i \qquad \text{for} \quad \alpha > \alpha_{min} \tag{25}$$

where α_{min} is the minimum solids fraction at which frictional transfer becomes influential. Experimental observations indicate that the frictional normal stress increases rapidly with bulk density and diverges as α_0 is approached. A simple algebraic representation of this behavior is (cf. [18])

$$p_i^f = \frac{\alpha_i \rho_i}{\alpha_{tot}} Fr \frac{(\alpha - \alpha_{min})^p}{(\alpha_0 - \alpha)^n}. \tag{26}$$

where Fr is a material constant. The frictional viscosity, μ_i^f, is related to the frictional pressure and the angle of internal friction, ϕ

$$\mu_i^f = \frac{p_i^f \sin(\phi)}{2\sqrt{I_2}} \tag{27}$$

where I_2 denotes the second invariant of the strain rate tensor. Following [20], the total stress is taken as the sum of the contributions from the separate mechanisms, each evaluated as though it acted alone

$$\boldsymbol{\sigma}^{tot} = \boldsymbol{\sigma}^f + \boldsymbol{\sigma}^c \tag{28}$$

where the superscript c indicates both collisional and kinetic contributions. However, in the production term of Eq. (10), the frictional terms are deleted corresponding to assuming that the frictional work is directly converted to thermal internal energy.

The numerical method for obtaining transient solutions is discussed in detail in [12]: the time discretization is based on a first order predictor-corrector method while spatial discretization is based on a second order flux-limited finite volume method. Linear solvers are based on whole-field methods [21].

3 RESULTS

3.1 Homogeneously sheared mixture

Savage and Sayed [22] have measured the normal and shear stresses developed by granular materials in a shear flow cell. These experiments are an excellent means of evaluating the solids stress part of the model. We focus here on binary mixtures as the single class case has been extensively discussed in [2]. The binary mixture consists of polystyrene beads (specific gravity 1.095) where $d_A = 0.55$ and $d_B = 1.68mm$, respectively with a restitution coefficient of 0.8. The solids fractions for the small and large particles constitute 30 and 70 percent of the total bulk solids volume fraction.

For the case of simple shear, the model presented above becomes a set of ordinary differential equations which have to be supplemented with boundary conditions on the solid surfaces of the shear cell. However, as the distribution of solids in the shear cell is unknown and the boundary conditions uncertain, we assume the velocity gradient to be uniform and equal for both particle classes. The system simplifies to two coupled algebraic equations for Θ_A and Θ_B, stating that production equals dissipation for each size class: $-\Sigma_{i,xy}\frac{du}{dy} + \gamma_i = 0$. Frictional transfer has been excluded from the present model. The present analysis differs from that in [6], since unequal granular temperatures are used here and a different radial distribution function is employed. Fig. 1 shows the comparisons of the present numerical solution of the set of equations and the experimental results for the mixture shear stress and the normal stress as function of the shear rate du/dy and of the bulk volume

fraction. Also shown are predictions with a single particle model using a mean particle diameter of $1.34mm$. Generally, for the lower solids fractions, both theories somewhat overpredict the stresses. At the highest bulk solids fraction, all stress components are, however, strongly underestimated which most likely indicates that the transfer of momentum becomes affected by friction, which was neglected in this specific case. The present, more general, binary model predictions are higher than the corresponding predictions in [6], owing to the separate granular temperatures for each class. At these diameter ratios (± 3), the temperatures do not equilibrate completely, leading to higher stress levels. The differences with the experimental data at lower solids bulk fraction are attributed to the assumption of Gaussian distributions and to the form of the radial distribution function to which the results are highly sensitive.

3.2 Particle pressure along the wall of a bubbling fluidized bed

To validate the solids pressure model and the code, a comparison was made with the experimental data of [23] reporting measurements of the solids pressure magnitude in a bubbling bed consisting of a square channel ($1.22 \times 0.127 \times 0.127m^3$), homogeneously fluidized with air. The bed is initially filled with glass beads ($d_p = 0.5mm.; \rho = 2500kg/m^3$), to a depth of 43 cm. As three dimensional calculations are very computationally intensive, the square channel was approximated by a flat two-dimensional geometry having a width equal to the size of the channel. Calculations were performed at three conditions, i.e. at superficial gas-velocities of 0.4, 0.6 and 0.8 m/s. The grid consists of 36×96 points. Fig. 2 shows vertical profiles of the computed time-averaged (over left and right wall) solids pressure (kinetic plus frictional) along the wall, together with the experimental data of [23]. Considering the geometric approximation, the agreement is reasonable, demonstrating an increase of solids pressure with height caused by fluctuating particle motion as induced by bubble growth, and a decrease to zero at greater heights where the solids fraction vanishes. Furthermore, the calculated

profiles exhibit an increase in solids pressure as the superficial gas velocity is increased. Most of the solids pressure originates from the kinetic part, not from the frictional regime. The remaining discrepancies with the experimental data are primarily attributed to (i) an insufficient period of averaging causing scatter in the data and (ii) the geometric approximations made by simulating a two dimensional geometry which may change the bubble dynamics. A similar comparison was presented recently in [16], using a kinetic theory model, but excluding frictional stresses. Although the period of averaging was similar (9 sec), their results exhibit rather spiky profiles. Possibly, this is caused by the specification of a minimum granular temperature. As frictional stresses are included in the present model, specifying such a minimum is unnecessary.

3.3 Behavior of homogeneously fluidized beds

Most validation studies of granular flow models for fluidized beds deal with single bubble injection (e.g. [16]). Generally, kinetic theory models reproduce well the qualitative features of these geometries. The present study focuses on the global behavior of homogeneously fluidized beds, as these are to be used for the biomass pyrolysis. The fluidized bed studied is $0.68m$ wide, initially filled up to $0.4m$ with sand ($\rho_s = 2600kg/m^3, d_p = 0.5mm$) or with a sand-biomass mixture (2/3 sand 1/3 biomass volumetrically; biomass properties: $\rho_b = 700kg/m^3, d_p = 0.5mm$). All computations were performed on a 40×128 grid. In order to trigger bubbling, a disturbance was introduced in the initial volume fraction distribution.

The obtained fields are transient owing to hydrodynamic instabilities giving rise to spatial inhomogeneity. Fig. 3 shows a snapshot of the solids volume fraction and phase velocities at $t = 3$ s. Bubbles can be identified which form at the bottom of the bed and rise, growing through coalescence, in accordance with visual observations in the bubbly flow regime. Typical bubble shapes consist of spheres with an excluded wake at the bottom; also in accordance with experimental data

(cf. [4]). Time-averaged results (not shown) lead to a flow pattern with two symmetric circulation loops and a solid fraction distribution showing a reasonably uniform dense lower bed and a gradually more diluted upper region. The solids fraction is not homogeneous over the width of the bed, exhibiting higher values at the lower near-wall region, induced by the large scale circulation. All of the above phenomena are well-known features of bubbling beds (e.g. [24]).

Fig. 4 shows the time-averaged solids volume fraction (computed from data along the centerline) in the lower part of the bed as function of the superficial gas velocity, compared to an experimental correlation from [24]. Also shown is an equilibrium solution obtained from a balance between gravity, gas-pressure gradient and gas-solid drag, which represents a simplified model of a fluidized bed. The computed solids fraction agrees quite well with the experimental correlation although some scatter is present in the simulated data due to the restricted period of time averaging. It is also concluded that the average lower-bed solids concentration is well predicted by the assumption of steady homogeneous flow.

To investigate the differences between a binary and a monodisperse mixture, 2 computations are compared: i) using the present binary flow model with sand and biomass properties for the separate solids classes and ii) using a monodisperse model with volume fraction weighted particle properties. Qualitatively, the simulations exhibit very similar behavior. One important difference is however the predicted solids distribution. The different properties of the particles cause the particle mixture to segregate. A quantitative measure of segregation may be defined as $S = (0.2\alpha_s - 0.4\alpha_b)/(0.2\alpha_s + 0.4\alpha_b)$, being zero if no segregation is present and 1 or -1 for complete segregation.

Fig 5. shows instantaneous distributions of the solids fractions and of the segregation parameter in the bed at $t = 6$ sec. Though initially the solids are perfectly mixed, already at this short time scale, segregation of the mixture is significant on a local scale, S mostly ranging between -0.2 and 0.2 (negative inside bubbles, carrying biomass to the top of the bed). The segregation can also be

quantified by the y-coordinate of the centers of mass of the sand and biomass, which are shown in Fig 6 as a function of time. It is shown that already one or two seconds after startup, segregation is significant and tends to increase with time. Segregation was found to increase when the size of the biomass particles was decreased, due to a greater difference in terminal velocity. The monodisperse simulation is clearly unable to predict any of these features and would only be useful for establishing the general flow patterns.

4 CONCLUSIONS

In this paper we have presented a new comprehensive model for the mathematical description of gas particle mixtures containing multiple solids classes based on a kinetic theory approach. The model has been applied to three different testcases in order to quantify its predictive capabilities. Comparison of predictions of the shear and normal stress components in a simple shear flow of a binary mixture reveal that for the lower bulk fractions, the stresses are somewhat overpredicted, whereas for the higher bulk fractions they are underpredicted, attributed to the neglect of frictional transfer in this testcase. A comparison has been made for the time-averaged particle pressure along the wall of a bubbling fluidized bed for different values of the superficial gas velocity. Predictions are generally in reasonable agreement with the available experimental data, exhibiting a rise of the particle pressure as function of the height induced by bubble growth and a rise of particle pressure at higher gas velocities. Predictions have been presented for a homogeneously aerated bed both with sand particles and with a sand-biomass mixture. For the monodisperse case, predictions of the solids volume fraction in the lower part of the bed have been compared to an experimental correlation and agreement is fairly good. Computations of a mixture of sand and biomass have shown that the qualitative behavior of the flow is not changed. The binary mixture model predicted a significant

amount of segregation, even during the short timespan here investigated. Considering the qualitative and reasonable quantitative agreement, this approach appears to be viable for further investigating the more complex situation of a reactive sand-biomass mixture.

ACKNOWLEDGMENT

This research was conducted at the Jet Propulsion Laboratory (JPL) and sponsored by the U.S. Department of Energy (DOE), with Mr. Neil Rossmeisel (DOE Headquarters) and Mr. D. Hooker (DOE Golden Center) serving as contract monitors, under an agreement with the National Aeronautics and Space Administration. Computational resources were provided by the supercomputing facility at JPL.

References

[1] Jenkins, J. T. and Savage, S. B., *J. Fluid Mech.* 130:187-202 (1983).

[2] Lun, C. K. K., Savage, S. B., Jeffrey, D. J. and Chepurniy, N., *J. Fluid Mech.* 140:223-256 (1984).

[3] Jenkins, J. T. and Richman, M. W., *Arch. Ration. Mech. Anal.* 87:355-377 (1985).

[4] Balzer, G. and Simonin, O. Extension of Eulerian Gas-Solid Flow Modelling to Dense Fluidized Bed. EDF Technical Report No. HE-44/93.13 B.

[5] Ding, J. and Gidaspow, D., *AIChE Journal* 36(4):523-538 (1990).

[6] Farell, M., Lun, C. K. K and Savage, S. B., *Acta Mechanica* 63:45-60 (1986).

[7] Jenkins, J. T. and Mancini, F., *Journal of Applied Mechanics.* 54:27-34 (1987).

[8] Jenkins, J. T. and Mancini, F., *Phys. Fluids A* 1(12):2050-2057 (1989).

[9] Zamankhan, P. *Phys. Rev. E* 52(5):4877-4891 (1995).

[10] Valiveti, P. and Koch, D. L., *Appl. Sci. Res.* 58:275-303 (1998).

[11] Drew, D. A., *Ann. Rev. Fluid Mech.*15:261-291 (1983).

[12] Lathouwers, D. and Bellan, J., Western States Section meeting of the Combustion Institute, Irvine, October 25-26, 1999.

[13] Chapman, S. and Cowling, T. G. 1970. *The Mathematical Theory of Nonuniform Gases.* Cambridge University Press.

[14] Goldman, E. and Sirovich, L., *Phys. Fluids* 10:1928-1940 (1967).

[15] Gidaspow, D., *Appl. Mech. Rev.* 39(1):1-22 (1986).

[16] Boemer, A. and Renz, U., *Int. J. Multiphase Flow.* 21(5):927-944 (1997).

[17] Ma, D., Eraslan, A. H. and Ahmadi, G., *Computers & Fluids* 22(1):25-50 (1993).

[18] Anderson, X and Jackson, R., *J. Fluid Mech.* 241:145-168 (1992).

[19] Syamlal, M. 1993. MFIX *Documentation Theory Guide.* DOE Report No. DOE/METC-94/1004.

[20] Johnson, P. C. and Jackson, R., *J. Fluid Mech.* 176:67-93 (1987).

[21] Lathouwers, D., *Modelling and Simulation of Turbulent Bubbly Flow.* PhD thesis, Delft University of Technology, The Netherlands, 1999.

[22] Savage, S. B. and Sayed, M. *J. Fluid Mech.* 142:391-430 (1984).

[23] Campbell, C. S. and Wang, D.G., *J. Fluid Mech* 227:495-508 (1991).

[24] Johnsson, F., Anderson, S. and Leckner, B., *Powder Technology* 68:117-123.

Figure Captions

Figure 1. Predictions of the total shear (left) and normal stresses (right) generated in a simple shear flow of a binary mixture as function of shear rate for various bulk solids fractions, compared with the experimental data from [22]. Predictions: —— binary model, - - - -, monodisperse model. Experimental data: ■: $\alpha_{tot} = 0.498$, ▲: $\alpha_{tot} = 0.512$, •: $\alpha_{tot} = 0.528$, ▼: $\alpha_{tot} = 0.542$.

Figure 2. Predictions of the total time-averaged solids pressure along the wall compared to experimental data of [23] at different superficial gas velocities. Predictions: $V_g = 0.4$: ——; $V_g = 0.6$: - - - ; $V_g = 0.8$:—·—, Experimental data: $V_g = 0.4$: ■; $V_g = 0.6$: , ▲; $V_g = 0.8$: •.

Figure 3. Instantaneous fields of the solid phase fraction (left), gas velocity (middle) and solids velocity (right) at $t = 3s$. (only 1 out of every 9 velocity vectors is shown).

Figure 4. Solid phase volume fraction in the lower bed as function of the superficial gas velocity: ■ present model, —— experimental correlation of [24], - - - equilibrium solution of two-fluid equations.

Figure 5. Instantaneous distributions of sand (left) and biomass (middle) concentrations, and of the segregation parameter (right) at $t = 6s$.

Figure 6. Time evolution of the y-coordinate of center of mass of sand and biomass compared to that of a monodispersed simulation: monodisperse:——, sand: - - - ; biomass: —·—.

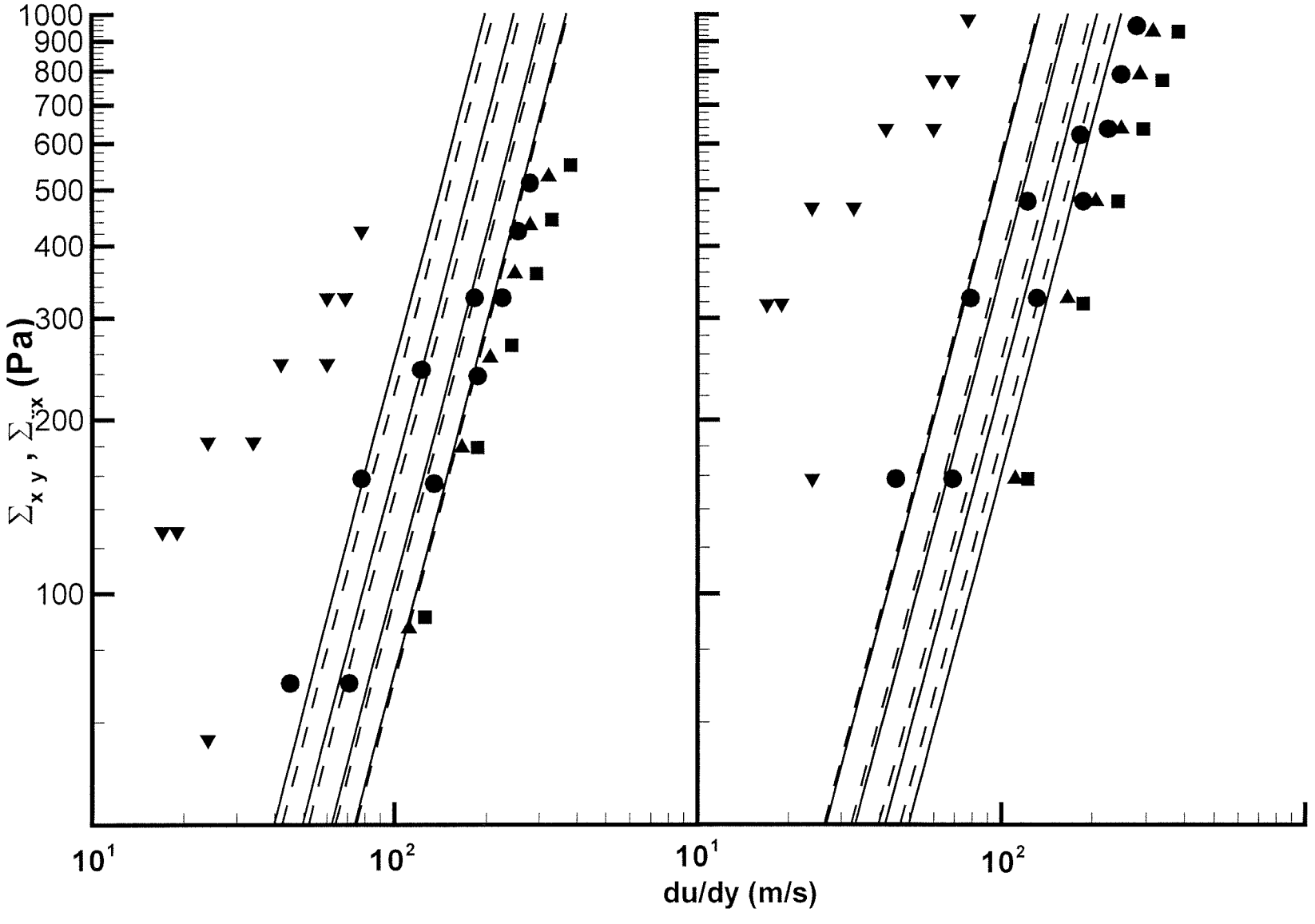
1000
900
800
700
600
500
400
300
200
100
$\Sigma_{x\,y}$, $\Sigma_{\ddot{y}x}$ (Pa)
10^1
10^2
10^1
10^2
du/dy (m/s)

Fig 1

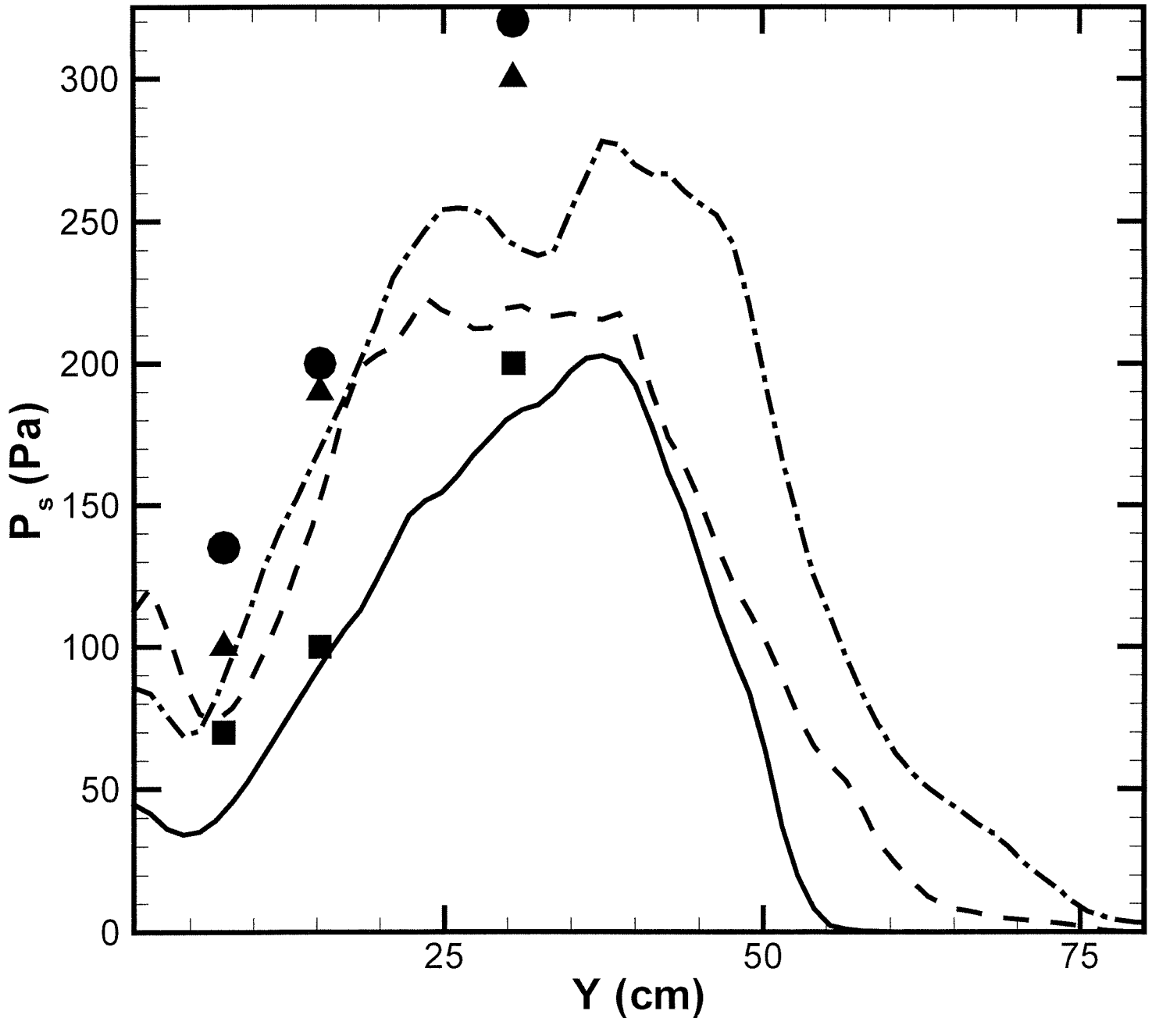

Fig 2

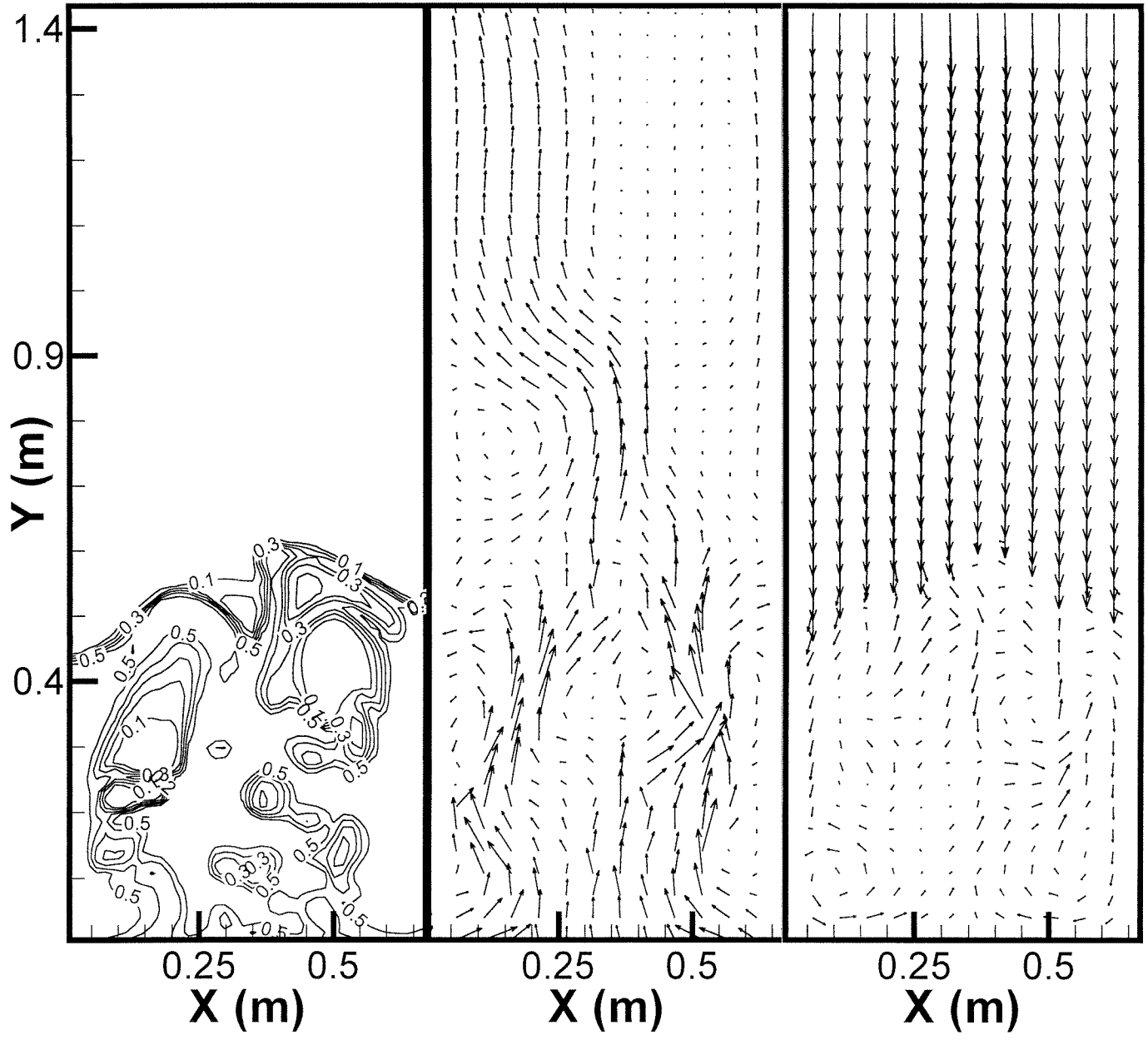

Fig 3

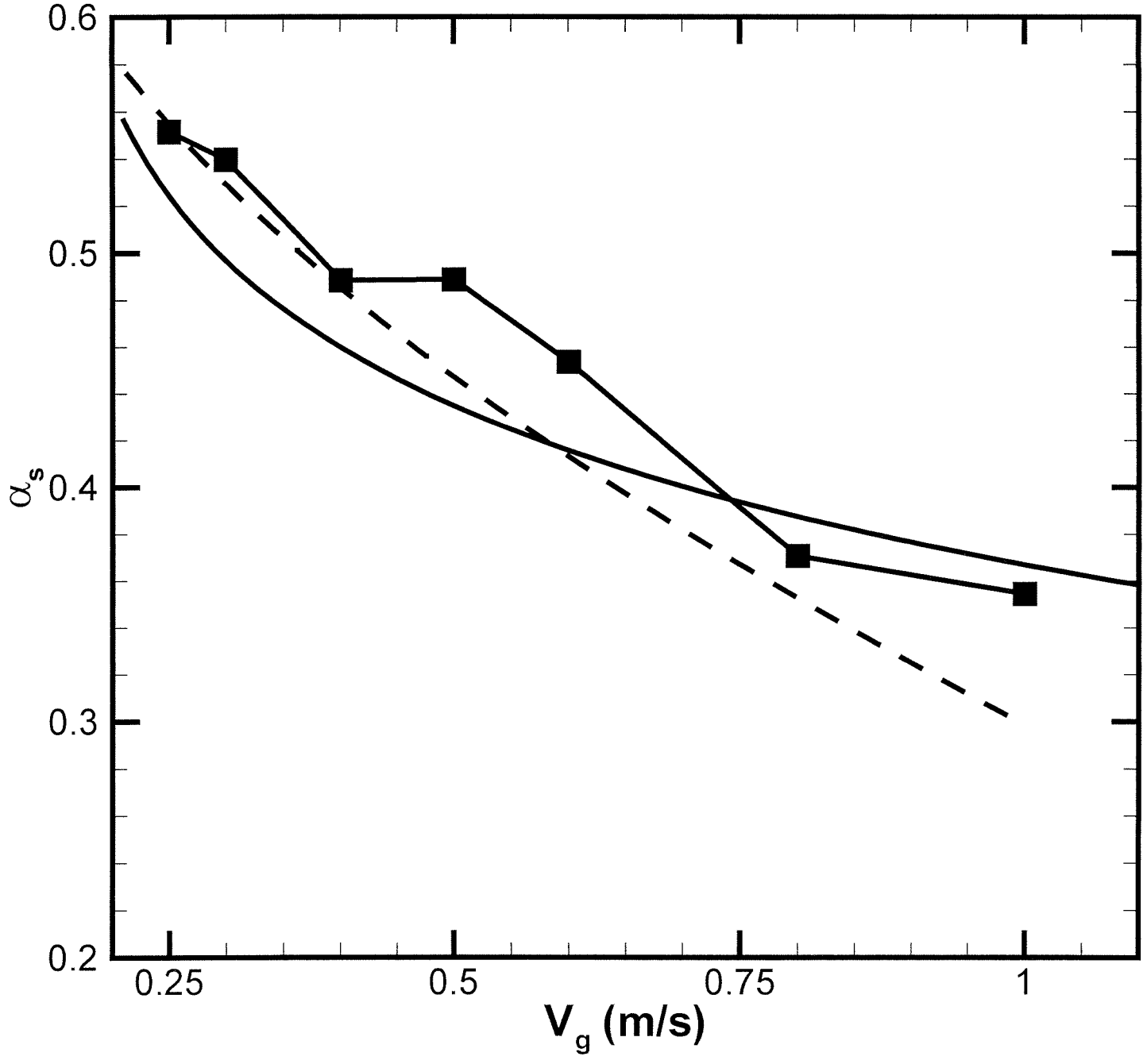

Fig 4

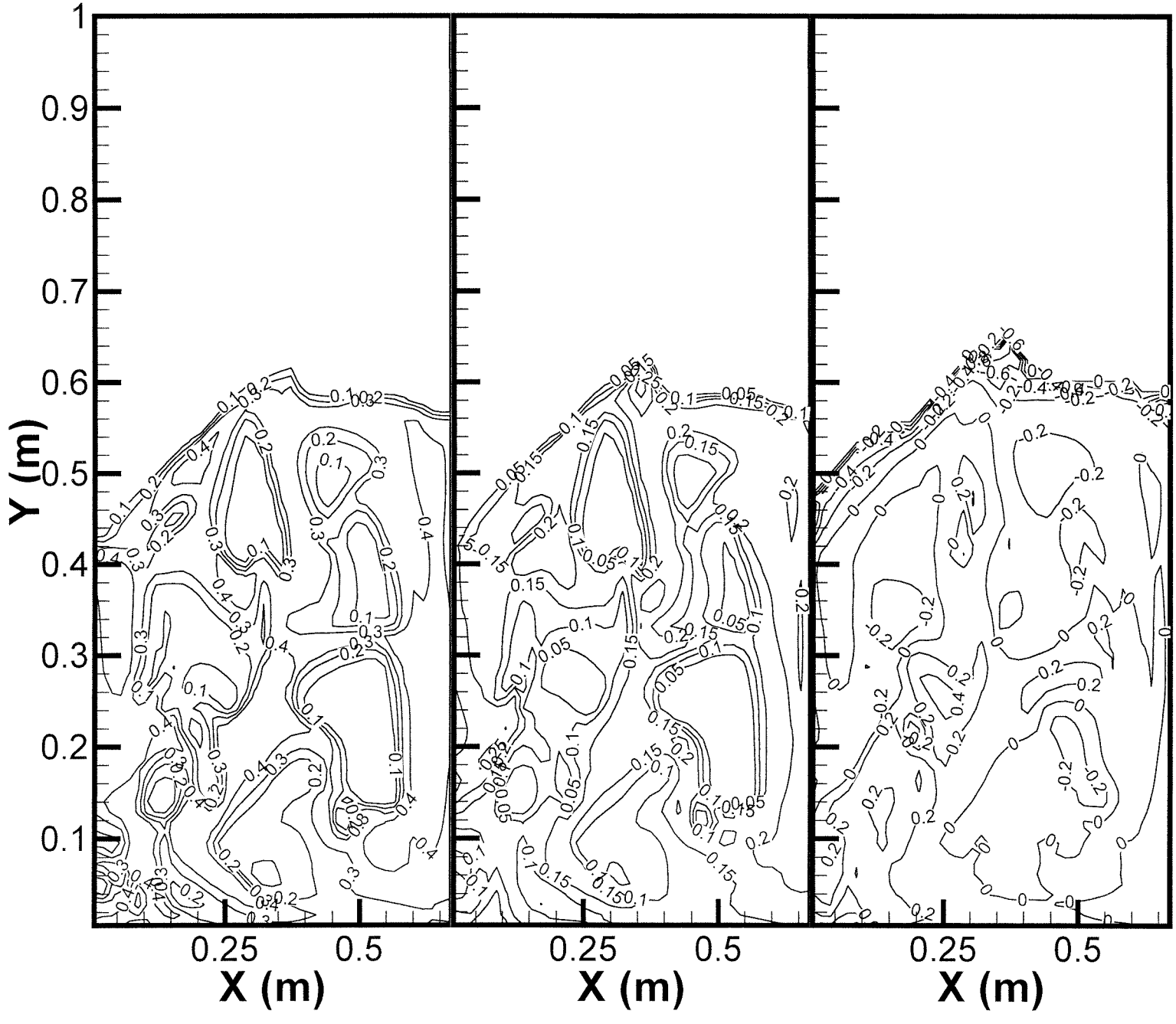

Figs-

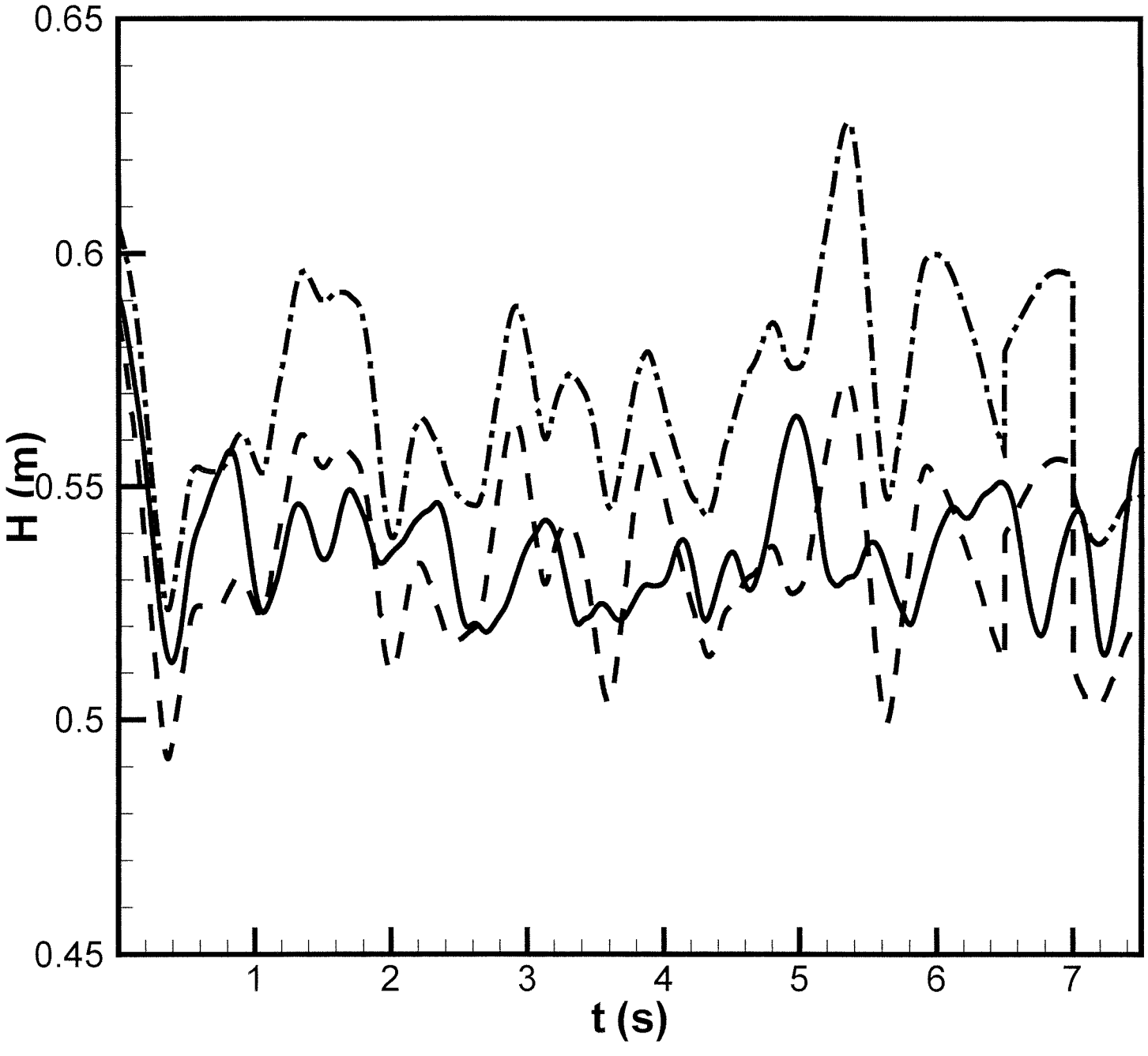

Fig 6